Nuclear Engineering and Technology 56 (2024) 1943–1949

Contents lists available at ScienceDirect

Nuclear Engineering and Technology

journal homepage: www.elsevier.com/locate/net

Original Article

A comparative study of 3D printing and sol-gel polymer production techniques: A case study on usage of ABS polymer for radiation shielding

Hasan Ogul [a,*], Batuhan Gultekin [a], Fatih Bulut [b], Hakan Us [a]

[a] *Department of Nuclear Engineering, Sinop University, Sinop, Turkey*
[b] *Scientific and Technological Research Applications and Research Center, Sinop University, Sinop, Turkey*

ARTICLE INFO

Keywords:
3D printer
Sol-gel
Radiation shielding
ABS polymer
Rare earth oxides

ABSTRACT

This study focuses on the comparative analysis of ABS polymer samples produced using two distinct manufacturing techniques: 3D printing and the sol-gel methods. In the first approach, ABS polymer was augmented with rare earth oxides, Er_2O_3 and Gd_2O_3, in nano powder form and fabricated into test specimens using 3D printing technology. In the second approach, identical samples were prepared via the sol-gel technique involving mold-based fabrication. Elemental content analysis revealed no significant differences between the samples produced by the two methods. The study proceeds to evaluate the gamma-ray shielding, neutron shielding, temperature resistance, and SEM/EDS pictures of ABS samples generated through both techniques. 3D printing method exhibited more favorable results in terms of structure morphology and thermal stability while there is no significant difference for radiation shielding. The results provide insights into the performance and suitability of each production method for radiation shielding applications. This research not only contributes to enhancing radiation shielding technology but also informs the selection of the most appropriate fabrication method for specific applications in nuclear technologies and diagnostic energy range in medical purposes.

1. Introduction

In the ever-evolving landscape of materials science, the development of innovative solutions for radiation shielding is of paramount importance. Ionizing radiation is integral to diverse applications, encompassing nuclear technology, medical diagnostics, and space exploration. This diversity underscores the pressing need for effective radiation shielding materials. In this context, polymer materials have found widespread utility across various industries due to their versatile properties, encompassing mechanical strength, chemical resistance, and cost-effectiveness [1]. Especially, Acrylonitrile Butadiene Styrene (ABS) material is one of the polymers mostly used in 3D printing technology. Among polymer materials, ABS has emerged as a material of particular interest, owing to its diverse range of applications, including 3D printing technology, automotive components, consumer electronics, and medical devices.

Recent research endeavors have been directed towards further enhancing ABS properties, particularly in the domains of radiation shielding. The incorporation of rare earth elements into polymer matrices has emerged as a promising avenue for tailoring advanced materials with improved characteristics. In this context, two prominent manufacturing techniques have garnered attention: 3D printing and the sol-gel methods. These methods offer unique advantages and have been subjects of extensive research in recent years. Our study aims to contribute to this evolving field by conducting a comprehensive comparative analysis of ABS polymer samples manufactured using these two techniques.

To provide context for the discussion, several influential studies in the field of radiation shielding deserve mention. Chang et al. [2] reviewed detailly new emerged manufacturing and evaluation strategies for radiation shielding: They present fruitful discussions on different polymer material manufacturing and recommend the produced polymers for biomedical applications. Besides, Elsafi et al. [3] have explored the potential of 3D-printed ABS and PLA composites filled with macro and nano-sized bismuth particles for radiation shielding. Their work highlights the growing interest in 3D printing technologies for radiation protection. Jreije et al. [4] focused on creating 3D filaments (PETG, ASA, NYLON, ULTRAT, PLA and ABS) filled with micron sized TiO_2 particles for shielding in medical radiation conditions. They reported that newly produced ABS composites could be effectively used to protect electronics

* Corresponding author.
E-mail address: hsnogul@gmail.com (H. Ogul).

https://doi.org/10.1016/j.net.2024.01.001
Received 8 December 2023; Received in revised form 27 December 2023; Accepted 1 January 2024
Available online 2 January 2024

Table 1
The components of the proposed materials.

Sample Code	ABS (%)	Gd_2O_3 (%)	Er_2O_3 (%)	Density (g/cm^3)
P-ABS-0	100	–	–	1.0442
P-ABS-Er10Gd5	85	5	10	1.1843
P-ABS-Er5Gd10	85	10	5	1.1829
M-ABS-0	100	–	–	1.0501
M-ABS-Er10Gd5	85	5	10	1.2080
M-ABS-Er5Gd10	85	10	5	1.2066

working in a radiotherapy room. In addition to these, Botero-Valencia et al. [5] have studied on design and application of radiation shields prepared with 3D technique for environmental sensors. They reported that the produced shield could be equal to the performance of known commercial brands.

Conversely, sol-gel synthesis offers a distinct avenue for material development. Avcioglu et al. [6] delved into the sol-gel technique in their research on radiation shielding materials by embedding B_4C particles in LDPE matrix. They found that addition of B_4C improves the neutron shielding capability of the LDPE polymer. Moreover, Sallam et al. [7] conducted a study on sol-gel-derived radiation shielding materials using $Ni_{0.5}Zn_{0.5}Fe_2O_4$ nanoparticles, expanding the repertoire of sol-gel applications in radiation protection. Addition of the mentioned nano particles improved the gamma-ray shielding capability of the polyethylene terephthalate polyester. Besides, ABS pellets were dissolved in acetone and boron nitride powders added in solution by Woosley et al. [8]. Then, they have explored the structure and neutron shielding performance of the prepared polymer materials. A significant increase in the radiation shielding characteristics was reported. In another report, Mostafa et al. [9] delved into the enhancement of radiation shielding properties in PVA polymer through the incorporation of rare earth elements (dysprosium (III) oxide and erbium (III) oxide). They reported that the samples with erbium oxide have better gamma-ray shielding capacity. Additionally, Brown et al. [10] mixed some rare earth oxides (Sm_2O_3, Eu_2O_3 and Gd_2O_3) into HDPE and theoretically highlighted X-ray shielding performance of them. They reported great potential of the prepared polymers to be utilized as an efficient X-ray shields in actual applications. Additionally, Hui et al. [11] provided an insightful overview of advances in rare earth composite shielding materials, offering critical insights into the materials' evolution.

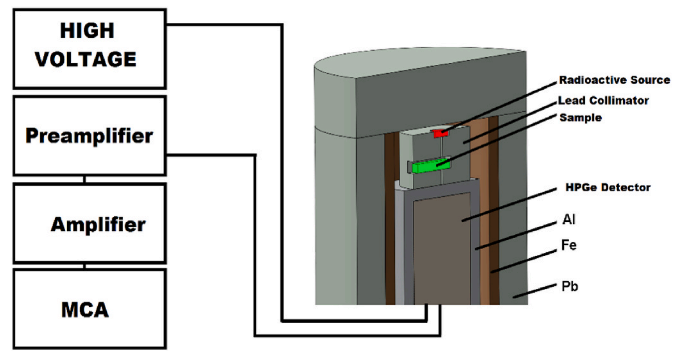

Fig. 3. HPGe detector measurement design.

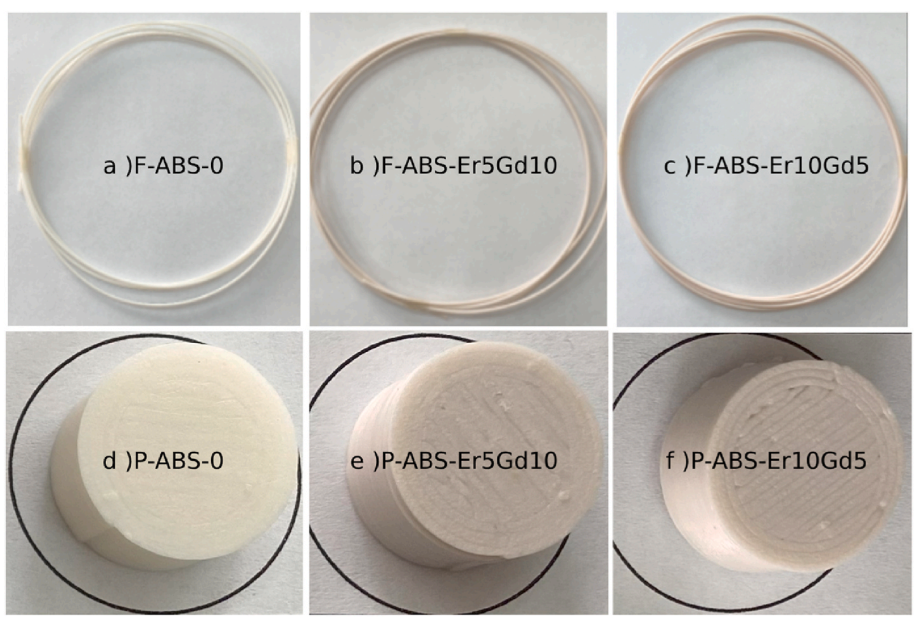

Fig. 1. The fabricated filaments and printed samples.

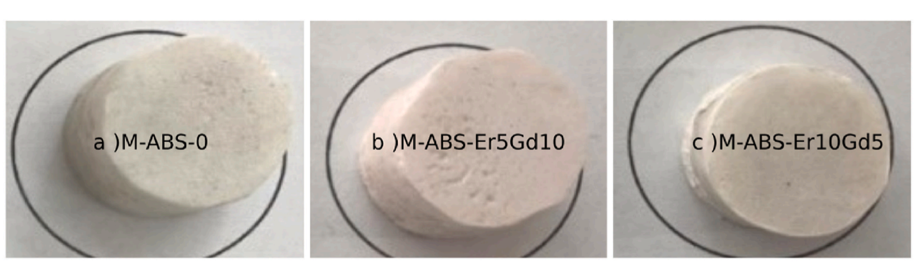

Fig. 2. The pictures of polymer samples produced via sol-gel technique.

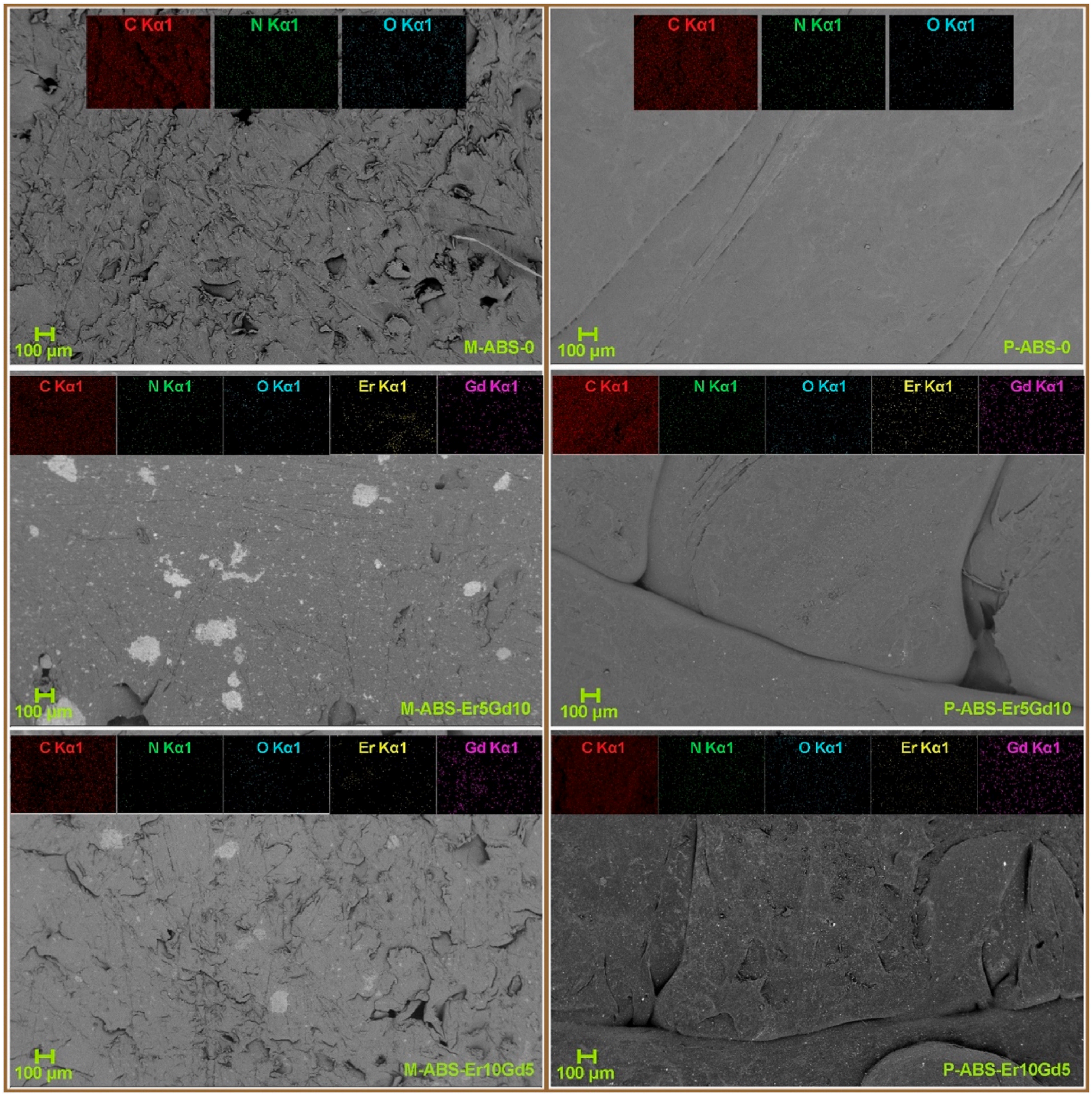

Fig. 4. The SEM images and EDS mappings of M-and P- series.

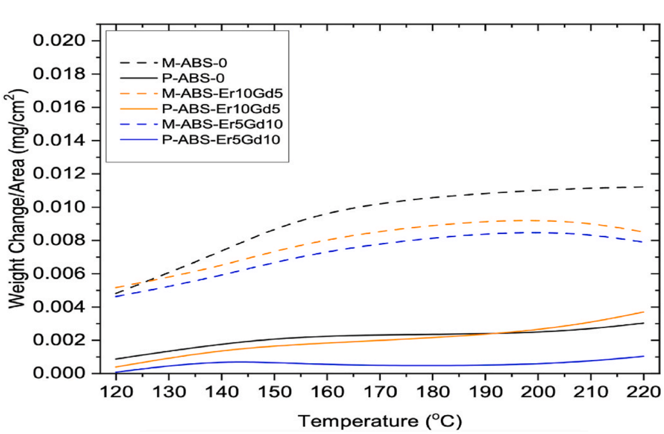

Fig. 5. The weight changes for each produced sample in response to temperature variation.

Collectively, these references underscore the significance of our research within the broader context of polymer modification and advanced materials development. Our study aims to provide valuable insights into the comparative performance of 3D-printed and sol-gel-produced ABS polymer samples, contributing to ongoing efforts to enhance the properties of this versatile material. The objective of this study is to provide a comprehensive comparative analysis of Erbium and Gadolinium-infused ABS polymers manufactured through 3D printing and sol-gel techniques in terms of gamma-ray and neutron shielding. Through a rigorous assessment encompassing Thermogravimetric Analysis (TGA), Scanning Electron Microscopy (SEM), Energy Dispersive X-ray Spectroscopy (EDS), and radiation shielding effectiveness, this research aims to elucidate the strengths and limitations of each manufacturing method.

2. Materials and methods

The materials selected for the presented work include ABS (a thermoplastic polymer), Er_2O_3 and Gd_2O_3 (rare earth oxides), and pure acetone (a solvent). ABS, with a density of 1.05 g/cm^3, stands out as a

Table 2
Mass attenuation coefficient (cm^2/g) results for the prepared samples.

Energy (keV)	M-ABS-0			M-ABS-Er5Gd10			M-ABS-Er10Gd5		
	Exp. (±stat.)	WinXCOM	FLUKA	Exp. (±stat.)	WinXCOM	FLUKA	Exp. (±stat.)	WinXCOM	FLUKA
59.5	0.1828 ± 0.0171	0.1885	0.1888	1.8707 ± 0.0146	1.9010	1.8555	1.7778 ± 0.0168	1.8140	1.7954
80.9	0.1745 ± 0.0135	0.1727	0.1728	0.9187 ± 0.0086	0.9351	0.9365	0.8640 ± 0.0111	0.8948	0.8960
276.3	0.1146 ± 0.0073	0.1187	0.1188	0.1374 ± 0.0142	0.1431	0.1431	0.1357 ± 0.0176	0.1413	0.1412
302.8	0.1088 ± 0.0139	0.1147	0.1148	0.1256 ± 0.0139	0.1333	0.1332	0.1302 ± 0.0095	0.1319	0.1317
356	0.1090 ± 0.0133	0.1079	0.1079	0.1258 ± 0.0086	0.1191	0.1191	0.1282 ± 0.0174	0.1181	0.1179
383.8	0.0998 ± 0.0152	0.1048	0.1048	0.1160 ± 0.0158	0.1135	0.1135	0.1193 ± 0.0106	0.1127	0.1126
511	0.0865 ± 0.0085	0.0932	0.0933	0.0961 ± 0.0092	0.0962	0.0963	0.0974 ± 0.0106	0.0958	0.0958
661.6	0.0798 ± 0.0173	0.0833	0.0834	0.0801 ± 0.0079	0.0839	0.0838	0.0859 ± 0.0180	0.0837	0.0836
1173.2	0.0598 ± 0.0178	0.0635	0.0636	0.0596 ± 0.0171	0.0624	0.0624	0.0595 ± 0.0150	0.0623	0.0626
1274.5	0.0597 ± 0.0159	0.0608	0.0609	0.0591 ± 0.0127	0.0597	0.0596	0.0608 ± 0.0185	0.0597	0.0596
1332.5	0.0593 ± 0.0142	0.0595	0.0595	0.0591 ± 0.0163	0.0583	0.0583	0.0597 ± 0.0173	0.0583	0.0583
Energy (keV)	P-ABS-0			P-ABS-Er5Gd10			P-ABS-Er10Gd5		
	Exp. (±stat.)	WinXCOM	FLUKA	Exp. (±stat.)	WinXCOM	FLUKA	Exp. (±stat.)	WinXCOM	FLUKA
59.5	0.1805 ± 0.0185	0.1885	0.1880	1.8667 ± 0.0126	1.8140	1.8011	1.7854 ± 0.0121	1.9010	1.8880
80.9	0.1628 ± 0.0153	0.1727	0.1725	0.8274 ± 0.0116	0.8948	0.8940	0.8790 ± 0.0109	0.9351	0.9355
276.3	0.1102 ± 0.0103	0.1187	0.1187	0.1401 ± 0.0143	0.1413	0.1413	0.1415 ± 0.0105	0.1431	0.1431
302.8	0.1057 ± 0.0163	0.1147	0.1147	0.1337 ± 0.0131	0.1319	0.1318	0.1246 ± 0.0106	0.1333	0.1301
356	0.1017 ± 0.0086	0.1079	0.1078	0.1238 ± 0.0186	0.1181	0.1181	0.1224 ± 0.0165	0.1191	0.1189
383.8	0.1068 ± 0.0088	0.1048	0.1047	0.1148 ± 0.0136	0.1127	0.1126	0.1164 ± 0.0187	0.1135	0.1135
511	0.0895 ± 0.0123	0.0932	0.0935	0.0892 ± 0.0198	0.0958	0.0958	0.0931 ± 0.0095	0.0962	0.0962
661.6	0.0844 ± 0.0176	0.0833	0.0835	0.0783 ± 0.0146	0.0837	0.0837	0.0793 ± 0.0200	0.0839	0.0838
1173.2	0.0586 ± 0.0166	0.0635	0.0638	0.0607 ± 0.0154	0.0623	0.0624	0.0607 ± 0.0115	0.0624	0.0623
1274.5	0.0613 ± 0.0078	0.0608	0.0608	0.0632 ± 0.0162	0.0597	0.0597	0.0566 ± 0.0176	0.0597	0.0596
1332.5	0.0580 ± 0.0178	0.0595	0.0595	0.0603 ± 0.0100	0.0583	0.0584	0.0602 ± 0.0123	0.0583	0.0583

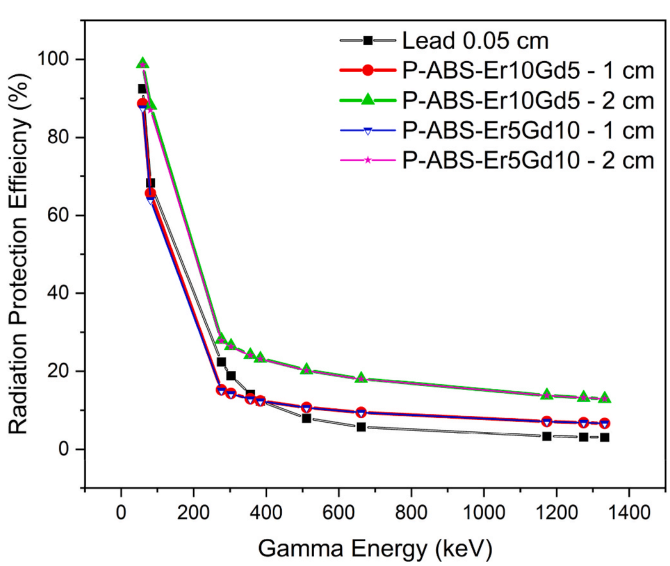

Fig. 6. Radiation protection efficiency graphs obtained by FLUKA.

superior polymer material due to its exceptional durability, mechanical properties, and resistance to chemicals. It typically melts within the range of 210–250 °C and solidifies when cooled, forming a robust structure that makes it well-suited for 3D printing technology, which is the focus of this study. The ABS granules used in this work were procured from RIIZ company in Kayseri, Turkey.

The chosen additive rare earth materials, Er_2O_3 (density: 8.64 g/cm^3) and Gd_2O_3 (density: 7.41 g/cm^3), were obtained in nanoparticle size (110 nm) with a purity of 99.95 % from Nanografi Company in Turkey. In particular, gadolinium is known for its effectiveness in thermal neutron shielding, but it is expected that these materials will improve the gamma-ray and neutron attenuation capabilities of the chosen polymer due to their high densities. Pure acetone, a colorless solvent with the chemical formula $(CH_3)_2CO$, was chosen for its cost-effectiveness and easy accessibility. It has a remarkable ability to dissolve ABS polymer and can be readily evaporated from the polymer solution. The acetone used in this study was also purchased from RIIZ company in Kayseri, Turkey.

The following sections provide details on the used production methods (sol-gel and 3D printing), and the resulting samples are identified with "F-", "P-", and "M-" tags for ease of differentiation. "F-", "P-", and "M-" correspond to "Filament," "Printed," and "Molded." Subsequently, the "P-" and "M-" tagged samples undergo evaluation through

Table 3
Transmitted neutron numbers on FLUKA simulation package and effective neutron removal cross-sections calculated theoretically.

Sample	Initial Neutron Numbers	Thermal Neutron (0.025 eV)	Fast Neutron (4.5 MeV)	Fast Neutron (4.5 MeV)
		Transmitted Neutron Numbers (FLUKA)	Transmitted Neutron Numbers (FLUKA)	Effective Neutron Removal Cross Section (cm^{-1})
M-ABS-0	10000000	1530015	8452412	0.0990
P-ABS-0	10000000	1540437	8462274	0.0984
M-ABS-Er10Gd5	10000000	86	8447616	0.0996
P-ABS-Er10Gd5	10000000	91	8476871	0.0976
M-ABS-Er5Gd10	10000000	0	8451797	0.0995
P-ABS-Er5Gd10	10000000	0	8479799	0.0975
Paraffin	10000000	446207	8105696	0.1224
Ordinary Concrete	10000000	6935829	8859970	0.0542

SEM/EDS, thermal and shielding analyses.

2.1. Filament and sample production

In this step, a twin-screw extrusion machine from Gulnar Machines in Turkey was utilized, featuring a screw diameter of 16 mm and an L/D ratio of 40. Filament production, incorporating nanoparticles, was carried out by referencing the values in Table 1. It is important to note that both ABS granules and the selected nanopowders underwent a drying process in an oven at 100 °C for 12 h before production. The filament diameters of ABS-0, ABS-Er10Gd5, and ABS-Er5Gd10 were found to be as 1.75 mm with a diameter tolerance of ±0.04 mm. Given that the average diameter of commercially available filaments is 1.75 mm, these produced filaments are well-suited for use in standard commercial polymer 3D printers. Subsequently, the fabricated filament tiles were employed to 3D print in order to create test samples with dimensions of 20 mm diameter and 10 mm thickness using a Creality CR-10 Smart Pro 3D Direct Drive printer. Fig. 1 displays the produced filaments and samples. The sample densities were determined with help of the Archimedes method [12].

2.2. Sol-gel technique and casting stage

The sample production process follows a specific sequence of stages. Initially, a precise amount of the polymer granules is carefully weighed. To ensure a high-quality solution, 200 mL of pure acetone is added to 100 g of ABS granules. These measured ABS granules and the pure acetone are combined in a tightly sealed jar to prevent solution evaporation. This mixture is left undisturbed for 24 h, allowing the ABS to fully dissolve. Subsequently, a magnetic stirrer is employed for 15 min to ensure the uniformity of the resulting viscous solution and to enhance its consistency. Nanopowders are introduced into the solution and subjected to magnetic stirring for 30 min. Finally, the mixture is poured into stainless-steel molds, each measuring 10 mm in thickness and 20 mm in diameter. The resulting samples are designated as M-ABS0, M-ABS-Er5Gd10 and M-ABS-Er10Gd5. Fig. 2 illustrates the produced samples. The average densities of these molded samples are determined using the Archimedes method [12].

2.3. Structure analyses

The incorporation and dispersion of Er_2O_3 and Gd_2O_3 nanoparticles within the ABS polymer matrix were visualized using a scanning electron microscope (JEOL, JSM-5300 model). In order to capture microscopic images of the samples, they underwent a coating process with a gold-palladium alloy within a vacuum environment. These images were taken at a resolution of 100 μm (μm). Additionally, an EDS point mapping analysis was carried out to assess whether the additive materials were evenly distributed throughout the samples. These structural analyses were conducted for both the M-and P- tagged samples, and the results obtained were subsequently compared to each other.

2.4. Thermal analysis

Mass changes for each produced sample in response to temperature were analyzed using a drying oven and a precision scale. These analyses involved subjecting the samples to constant temperatures of 120, 140, 160, 180, 200, and 220 °C for 10 min each, and then comparing the mass changes at each temperature to their original, unexposed mass. The assessment began at 110 °C since it represents the average bed temperature of 3D printers. As ABS has a melting temperature range of 210–250 °C, the maximum temperature was set at 220 °C.

2.5. Radiation shielding analysis

Radiation shielding analyses can be divided into two primary stages: the analysis of gamma-ray shielding and neutron shielding. Gamma-ray shielding analysis involves a combination of experimental measurements using a High Purity Germanium detector (HPGe), theoretical calculations with the WinXCOM [13] software, and Monte Carlo simulation (FLUKA [14]). Conversely, neutron shielding analysis primarily depends on theoretical calculations, specifically the effective removal cross-section, and Monte Carlo simulations using FLUKA, as there is a lack of experimental equipment available at our institution for neutron analysis. Many published studies could be listed with the usage of WinXCOM and FLUKA techniques [15–21]. The consistency of these programs with MCNP6 was previously reported in Ref. [22].

For the gamma-ray shielding experiments, the experimental setup is depicted in Fig. 3, which comprises an HPGe detector system, collimators and radioactive sources. The sample is positioned between the point source and the detector, precisely 3 cm away from the source and 3.9 cm away from the detector. A visual representation of this experimental setup is provided in Fig. 3. The point sources utilized include ^{241}Am (emitting radiation at 59.5 keV), ^{133}Ba (emitting radiation at 80.9, 276.3, 302.8, 356.0, and 383.8 keV), ^{22}Na (emitting radiation at 511.0 and 1274.5 keV), ^{137}Cs (emitting radiation at 661.6 keV), and ^{60}Co (emitting radiation at 1173.2 and 1332.5 keV). In the Monte Carlo simulation, we model the experimental setup and assign the mentioned energies to 10, 000, 000 monoenergetic gamma-rays. The parameters we consider for gamma-ray shielding analysis are the mass attenuation coefficient (MAC, μ/ρ) and the radiation protection efficiency (RPE). These parameters are distinct and serve to evaluate and discuss the gamma-ray shielding capabilities of the produced samples. The mathematical definitions of these parameters are provided in Equations (1) and (2).

$$MAC = \left(\frac{\ln(I_0/I)}{x}\right) \Big/ \rho_{shield}, \text{ in unit of cm}^2 \Big/ \text{g} \quad (1)$$

$$RPE = \left(1 - \frac{I}{I_0}\right) \times 100 \quad (2)$$

where ρ_{shield} and x and correspond to the shielding material density and thickness while the I and I_0 represent the densities of transmitted and incident radiation, respectively.

In the assessment of neutron shielding capabilities for the produced samples, we employ theoretical calculations of the effective removal cross-section. This approach is particularly suitable for evaluating fast neutron shielding. The mathematical expression for this calculation is presented in Equation (3).

$$\Sigma_R = \Sigma_i \rho_i \left(\Sigma_{R/\rho}\right)_i \quad (3)$$

where ρ_i is the partial density of the elements. In addition to the theoretical evaluation, we conduct FLUKA simulations by creating models of the produced samples and including various neutron energies in the simulation package. We subject the samples to bombardment by 10, 000, 000 monoenergetic neutrons, simulating the passage of these neutrons through the samples. Ultimately, the simulation assessment of the samples is carried out for a range of neutron energies, including thermal neutrons.

3. Results and discussion

The study presented here conducts comparative analyses of two distinct techniques for producing polymer samples: Sol-gel and 3D printing. To evaluate the surface morphology and the distribution of additives, SEM and EDS analyses of the fabricated samples were carried out. SEM images were obtained at 100× magnification, and EDS mapping was employed to collect data from the entire sample surface. Fig. 4 illustrates the SEM and EDS findings for both M-(Sol-gel) and P- (3D-printed) tagged samples, accompanied by EDS mapping images. Notably, the M-ABS-0 sample exhibited deep voids on its surface, a characteristic not observed in the image of the P-ABS-0 sample. This distinction highlights a fundamental difference in the production methods, which also applies to the ABS samples with additives. While the surface roughness of the M-ABS-Er5Gd10 sample was lower than that of M-ABS-0, an increase in voids on the surface was observed in the M-ABS-Er10Gd5 sample. In contrast, the P- samples did not show similar voids on their surfaces produced by the sol-gel method, but voids between the fibers were present due to the nature of the printing process. The absence of voids on the fibers reduced surface roughness, ensuring a homogenous distribution of additive elements on the surface. Notably, the P-ABS-Er10Gd5 sample exhibited noticeable voids compared to the P-ABS-Er5Gd10 sample, which could be attributed to changes in the additive ratios. When examining the EDS results, a significant difference in the homogeneous distribution of additive elements on the surface was observed between the M-and P- series. A homogenous distribution of additive elements on the surface is advantageous for radiation protection, making it a preferred characteristic. In this context, it was found that samples produced using the 3D printing method exhibited more favorable results in terms of surface morphology compared to those produced using the sol-gel technique.

The second analysis conducted on the produced polymer samples involves assessing the weight changes of each sample in response to temperature. As previously mentioned, the samples were subjected to temperature exposure for a duration of 10 min using a drying oven. Subsequently, the mass changes were determined by employing a precision scale and comparing them to their initial unexposed masses. The results of this analysis are presented in Fig. 5. It can be concluded that the 3D-printed samples exhibit greater thermal stability within the selected temperature range when compared to the M- series samples. Notably, the P-ABS-Er5Gd10 sample demonstrates superior 'weight change per unit area' values, resulting in less weight loss.

The final analysis conducted on the presented materials is radiation shielding analysis. In this regard, gamma-ray analysis of the sample shields is carried out using an HPGe detector system, as previously mentioned. This analysis is enhanced by incorporating theoretical calculations and Monte Carlo simulations. Table 2 provides the results of mass attenuation coefficients and compares the calculated, simulated, and measured outcomes. The table includes both the experimental results (Exp.) and the associated statistical uncertainties ($\pm$stat.). The experimental results were obtained through three repetitions, and the average value for each energy is determined as the corresponding mass attenuation coefficient. The statistical uncertainty is calculated as the maximum deviation between the average value and the results of the three separate measurements. The maximum discrepancy between the experimental results and those obtained through FLUKA and WinXCOM is approximately 7 %. This suggests that the selected Monte Carlo simulation and theoretical calculation tools align closely with the experimental results. Additionally, it was found that the mass attenuation coefficient values decrease as the gamma energy increases, and the ABS-Er10Gd5 sample exhibits superior gamma-ray shielding capabilities. There is no significant difference observed between the M-and P- series samples; therefore, it would not be appropriate to claim one as superior to the other in terms of gamma-ray shielding.

In this study, a broad gamma-ray energy range has been selected, covering photons in the diagnostic energy range to the high-energy region, with the aim of identifying potential application areas for the proposed polymers. Based on the evaluation of mass attenuation coefficient results, the produced polymers with additives show promise for gamma-ray shielding in the diagnostic energy region. To assess their performance, radiation protection efficiencies are computed and compared with the results of a 0.5 mm thick lead material, as commercial lead thyroid shields commonly have this thickness. Fig. 6 illustrates this comparison, with simulated lead results compared to P-ABS-Er5Gd10 and P-ABS-Er10Gd5 samples at polymer material thicknesses of 1 cm and 2 cm. The results demonstrate that ABS samples with a 1 cm thickness provide similar gamma-ray protection to lead thyroid shields, while ABS samples with a 2 cm thickness offer enhanced shielding efficiency across all selected gamma-ray energies.

The final stage of shielding analysis for the produced samples focuses on assessing their neutron shielding capabilities. Initially, calculations are performed to determine the effective removal cross sections for fast neutrons. Subsequently, the number of transmitted neutrons through the prepared samples is calculated using the FLUKA simulation package. It is important to note that this section lacks experimental measurements due to the absence of appropriate equipment at the authors' home institution and budget constraints in the presented study. It is also worth emphasizing that hydrogen exhibits the highest fast neutron effective removal cross-section value. Therefore, the addition of Gd_2O_3 and Er_2O_3 is expected to reduce the hydrogen content in the ABS samples, potentially resulting in reduced fast neutron shielding capability compared to ABS-0 samples. Table 3 provides a summary of the obtained results. As observed, ABS-0 samples possess higher effective removal cross-sections compared to ABS-Er5Gd10 and ABS-Er10Gd5 samples, indicating superior fast neutron shielding ability in the case of ABS-0. Therefore, it is safe to state that the FLUKA simulation results are consistent with the outcomes of effective removal calculations. On the other hand, it is a well-established fact that gadolinium possesses the highest thermal neutron absorption cross-section among all elements. Therefore, ABS-Er5Gd10 is expected to be the most effective thermal neutron shielding material among the materials presented. Table 2 demonstrates that 100 % shielding of thermal neutrons is achieved at a sample thickness of 1 cm.

Furthermore, it is important to mention that while all the produced samples offer better fast neutron shielding capabilities than ordinary concrete, they do not perform as effectively as paraffin, which are common materials used for neutron shielding applications. Conversely, the ABS samples produced with additives demonstrate notable thermal neutron shielding capabilities in comparison to paraffin.

4. Conclusion

The presented study on comparison of 3D printing and sol-gel techniques proves that 3D printing technology offers better structure of radiation shielding samples and thermal stability compared to the sol-gel technique involving mold-based fabrication. It is found that the obtained 3D-printed samples are replaceable with toxic lead element in diagnostic energy range of medical applications. Besides, it should be underlined here that the proposed polymer samples are significantly effective on thermal neutron shielding but not on fast neutron shielding. The applications for thermal neutrons could be listed as thermal neutron activation analysis for biological samples and boron neutron capture therapy. These could be good place for the candidate materials.

This limitation can be overcome by employing layered shielding structures. For instance, a layer of paraffin could moderate fast neutrons and convert them into thermal neutrons which are emitted from a radiation source. Subsequently, a second layer, which can be printed using ABS-Er5Gd10 material, can shield these thermal neutrons effectively, making the combination suitable for both thermal and fast neutron shielding applications. The rapid and cost-effective production capability of these novel 3D-printed samples is expected to help the industry in prototyping essential radiation shielding materials, paving the way for more efficient and safer radiation protection solutions.

Declaration of competing interest

The authors declare that they have no known competing financial interests or personal relationships that could have appeared to influence the work reported in this paper.

Acknowledgements

This study was funded by the Scientific and Technological Research

Council of Turkey (TUBITAK) 1002-A Grant No 122M736.

References

[1] B. Gultekin, H. Ogul, Evaluation of Acrylonitrile Butadiene Styrene (ABS) polymer reinforced with Bi and TiO2 nanopowders for gamma and neutron shielding, Radiochim. Acta 111 (2) (2023) 137–145.
[2] Q. Chang, G. Shaoyun, X. Zhang, Radiation shielding polymer composites: ray-interaction mechanism, structural design, manufacture and biomedical applications, Mater. Des. (2023) 112253.
[3] M. Elsafi, M.A. El-Nahal, M.I. Sayyed, I.H. Saleh, M.I. Abbas, Novel 3-D printed radiation shielding materials embedded with bulk and nanoparticles of bismuth, Sci. Rep. 12 (1) (2022) 12467.
[4] A. Jreije, S.K. Mutyala, B.G. Urbonavičius, A. Šablinskaitė, N. Keršienė, J. Puišo, Z. Rutkūnienė, D. Adlienė, Modification of 3D printable polymer filaments for radiation shielding applications, Polymers 15 (7) (2023) 1700.
[5] J.S. Botero-Valencia, M. Mejia-Herrera, J.M. Pearce, Design and implementation of 3-D printed radiation shields for environmental sensors, HardwareX 11 (2022) e00267.
[6] S. Avcıoğlu, M. Buldu, F. Kaya, C.B. Üstündağ, E. Kam, Y.Z. Menceloğlu, H. Y. Kaptan, C. Kaya, Processing and properties of boron carbide (B4C) reinforced LDPE composites for radiation shielding, Ceram. Int. 46 (1) (2020) 343–352.
[7] F.H. Sallam, M. Tharwat, A.H. Almuqrin, M.I. Sayyed, K.A. Mahmoud, Ni0. 5Zn0. 5Fe2O4 nanoparticles reinforced polyester composite for advanced radiation shielding applications: a detailed discussion for synthesis, characterization, and gamma-ray attenuation properties, Radiat. Phys. Chem. 208 (2023) 110907.
[8] S. Woosley, N.A. Galehdari, A. Kelkar, S. Aravamudhan, Fused deposition modeling 3D printing of boron nitride composites for neutron radiation shielding, J. Mater. Res. 33 (22) (2018) 3657–3664.
[9] M.Y. Mostafa, H.M. Zakaly, S.A. Issa, H.A. Saudi, A.M.A. Henaish, Tailoring variations in the linear optical and radiation shielding parameters of PVA polymeric composite films doped with rare-earth elements, Appl. Phys. A 128 (3) (2022), 199.
[10] K. Saenboonruang, W. Poltabtim, A. Thumwong, T. Pianpanit, C. Rattanapongs, "Rare-earth oxides as alternative high-energy photon protective fillers in HDPE composites: theoretical aspects, Polymers 13 (12) (1930) 2021.
[11] H. Jing, L. Geng, S. Qiu, H. Zou, M. Liang, D. Deng, "Research progress of rare earth composite shielding materials, J. Rare Earths 41 (1) (2023) 32–41.
[12] M.E. Mahmoud, A.M. El-Khatib, M.S. Badawi, A.R. Rashad, R.M. El-Sharkawy, A. A. Thabet, Fabrication, characterization and gamma rays shielding properties of nano and micro lead oxide-dispersed-high density polyethylene composites, Radiat. Phys. Chem. 145 (2018) 160–173.
[13] L. Gerward, N. Guilbert, K.B. Jensen, H. Levring, WinXCom-a program for calculating X-ray attenuation coefficients, Radiat. Phys. Chem. 71 (3–4) (2004) 653–654.
[14] T.T. Böhlen, F. Cerutti, M.P.W. Chin, A. Fassò, A. Ferrari, P.G. Ortega, A. Mairani, P.R. Sala, G. Smirnov, V. Vlachoudis, The FLUKA code: developments and challenges for high energy and medical applications, Nucl. Data Sheets 120 (2014) 211–214.
[15] C.V. More, F. Akman, K. Dilsiz, H. Ogul, P.P. Pawar, Estimation of neutron and gamma-ray attenuation characteristics of some ferrites: geant4, FLUKA and WinXCom studies, Appl. Radiat. Isot. 197 (2023) 110803.
[16] F. Akman, H. Ozdogan, O. Kilicoglu, H. Ogul, O. Agar, M.R. Kacal, H. Polat, A. Tursucu, Gamma, charged particle and neutron radiation shielding capacities of ternary composites having polyester/barite/tungsten boride, Radiat. Phys. Chem. 212 (2023) 111120.
[17] I. Erkoyuncu, F. Akman, H. Ogul, M.R. Kaçal, H. Polat, I. Demirkol, K. Dilsiz, B. Ertuğral, A detailed investigation of gamma and neutron shielding capabilities of ternary composites doped with polyacrylonitrile and gadolinium (III) sulfate, Appl. Radiat. Isot. 196 (2023) 110789.
[18] H. Oğul, O. Agar, F. Bulut, M.R. Kaçal, K. Dilsiz, H. Polat, F. Akman, A comparative neutron and gamma-ray radiation shielding investigation of molybdenum and boron filled polymer composites, Appl. Radiat. Isot. 194 (2023) 110731.
[19] O. Kilicoglu, F. Akman, H. Ogul, O. Agar, U. Kara, Nuclear radiation shielding performance of borosilicate glasses: numerical simulations and theoretical analyses, Radiat. Phys. Chem. 204 (2023) 110676.
[20] H. Oğul, H. Polat, F. Akman, M.R. Kaçal, K. Dilsiz, F. Bulut, O. Agar, Gamma and Neutron Shielding Parameters of Polyester-based composites reinforced with boron and tin nanopowders, Radiat. Phys. Chem. 201 (2022) 110474.
[21] Hasan Ogul, Radiation attenuation properties of polymer composites mixed with tantalum carbide, Radiat. Eff. Defect Solid 177 (5–6) (2022) 531–544.
[22] T. Frosio, P. Bertreix, N. Menaa, S. Thomas, Calculation and benchmark of fulence-to-local skin equivalent dose coefficents for neutrons with FLUKA, MCNP, and GEANT4 monte-carlo codes, J. Radiol. Prot. 41 (3) (2021) 564–578.